REPORT DOCUMENTATION PAGE

1. REPORT DATE *(DD-MM-YYYY)*	2. REPORT TYPE	3. DATES COVERED *(From - To)*
30-05-2013	Journal Article	

4. TITLE AND SUBTITLE

Combined Effect of Reduced Band Number and Increased Bandwidth on Shallow Water Remote Sensing: The Case of WorldView 2

5a. CONTRACT NUMBER

5b. GRANT NUMBER

5c. PROGRAM ELEMENT NUMBER
N/A

6. AUTHOR(S)

ZhongPing Lee, Alan Weidemann, and Robert Arnone

5d. PROJECT NUMBER
NNH09AM26I

5e. TASK NUMBER

5f. WORK UNIT NUMBER
73-4223-01-5

7. PERFORMING ORGANIZATION NAME(S) AND ADDRESS(ES)

Naval Research Laboratory
Oceanography Division
Stennis Space Center, MS 39529-5004

8. PERFORMING ORGANIZATION REPORT NUMBER

NRL/JA/7330-12-1190

9. SPONSORING/MONITORING AGENCY NAME(S) AND ADDRESS(ES)

NASA Headquarters
Attn: Laurie Friederich
Mail Code 210.H, Bldg. 17, Rm. N111
Greenbelt, MD

10. SPONSOR/MONITOR'S ACRONYM(S)
NASA

11. SPONSOR/MONITOR'S REPORT NUMBER(S)

12. DISTRIBUTION/AVAILABILITY STATEMENT

Approved for public release, distribution is unlimited.

13. SUPPLEMENTARY NOTES

14. ABSTRACT

Simulated bidirectional reflectance distribution functions (BRDF) were compared with measurements made just beneath the water's surface. In Case I water, the set of simulations that varied the particle scattering phase function depending on chlorophyll concentration agreed more closely with the data than other models. In Case II water, however, the simulations using fixed phase functions agreed well with the data and were nearly indistinguishable from each other, on average. The results suggest that BRDF corrections in Case II water are feasible using single, average, particle scattering phase functions, but that the existing approach using variable particle scattering phase functions is still warranted in Case I water.

15. SUBJECT TERMS

oceanic optics, oceanic scattering, radiative transfer, passive remote sensing

16. SECURITY CLASSIFICATION OF:			17. LIMITATION OF ABSTRACT	18. NUMBER OF PAGES	19a. NAME OF RESPONSIBLE PERSON
a. REPORT	b. ABSTRACT	c. THIS PAGE	UL	16	Alan Weidemann
Unclassified	Unclassified	Unclassified			19b. TELEPHONE NUMBER *(Include area code)* (228) 688-6232

PUBLICATION OR PRESENTATION RELEASE REQUEST

Pubkey: 8214   NRLINST 5600.2

1. REFERENCES AND ENCLOSURES	2. TYPE OF PUBLICATION OR PRESENTATION	3. ADMINISTRATIVE INFORMATION
Ref: (a) NRL Instruction 5600.2 (b) NRL Instruction 5510.40D Encl: (1) Two copies of subject paper (or abstract)	( ) Abstract only, published ( ) Abstract only, not published ( ) Book ( ) Book chapter ( ) Conference Proceedings ( ) Conference Proceedings (refereed) (not refereed) ( ) Invited speaker ( ) Multimedia report (X) Journal article (refereed) ( ) Journal article (not refereed) ( ) Oral Presentation, published ( ) Oral Presentation, not published ( ) Other, explain	STRN NRL/JA/7330-12-1190 Route Sheet No. 7330/ Job Order No. 73-4223-01-5 Classification X U C Sponsor NASA approval obtained ____ yes X no

4. AUTHOR

Title of Paper or Presentation

The Combined Effect of Reduced Spectral Bands and Increased Bandwidth on Shallow Water Remote Sensing: The Case of WorldView 2

Author(s) Name(s) (First,MI,Last), Code, Affiliation if not NRL

ZhongPing Lee Univ. of MA Boston Alan D. Weidemann 7333 Robert A Arnone 7330

It is intended to offer this paper to the _____

(Name of Conference)

_____

(Date, Place and Classification of Conference)

and/or for publication in **Transactions on Geoscience and Remote Sensing,** Unclassified _____
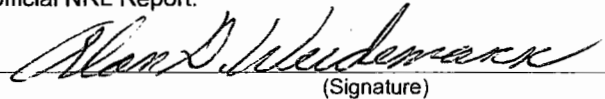
(Name and Classification of Publication)   (Name of Publisher)

After presentation or publication, pertinent publication/presentation data will be entered in the publications data base, in accordance with reference (a).
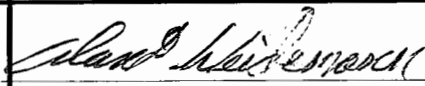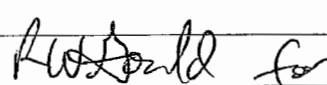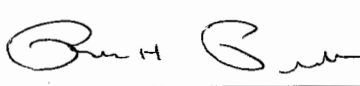
It is the opinion of the author that the subject paper (is ____) (is not ___X) classified, in accordance with reference (b).

This paper does not violate any disclosure of trade secrets or suggestions of outside individuals or concerns which have been communicated to the Laboratory in confidence. This paper (does ____) (does not ___X) contain any militarily critical technology.

This subject paper (has ____) (has never __X__) been incorporated in an official NRL Report.

Alan D. Weidemann, 7333	_(signature)_
Name and Code (Principal Author)	(Signature)

5. ROUTING/APPROVAL

CODE	SIGNATURE	DATE	COMMENTS
Author(s) Weideman	_Alan Weidemann_	16 Apr 2012	Need by ____ 03 May 12
			Publicly accessible sources used for this publication
Section Head N/A			
Branch Head Robert A Arnone, 7330	_R W Gould for_	4/16/12	
Division Head Ruth H. Preller, 7300	_signature_	4/16/12	1. Release of this paper is approved. 2. To the best knowledge of this Division, the subject matter of this paper (has ____) (has never __x__) been classified.
Security, Code 1231			1. Paper or abstract was released. 2. A copy is filed in this office.
Office of Counsel,Code 1008.3	_ABeede invention memo_	4/12/2012	
ADOR/Director NCST E. R. Franchi, 7000			
Public Affairs (Unclassified/ Unlimited Only), Code 7030.4	_Shannon Ireland_	4-23-12	
Division, Code			
Author, Code			

HQ-NRL 5511/6 (Rev. 12-98) (e)   THIS FORM CANCELS AND SUPERSEDES ALL PREVIOUS VERSIONS

12-1231-1431

PUBLICATION OR PRESENTATION RELEASE REQUEST

Subkey: NRLINST 5600.2

Ref: (a) NRL Instruction 5600.2
(b) NRL Instruction 5510.40D

Encl: (1) Two copies of subject paper
(or abstract)

( ) Abstract only, published
( ) Book
( ) Conference Proceedings
(refereed)
( ) Invited speaker
(X) Journal article (refereed)
( ) Oral Presentation, published
( ) Other, explain

( ) Abstract only, not published
( ) Book chapter
( ) Conference Proceedings
(not refereed)
( ) Multimedia report
( ) Journal article (not refereed)
( ) Oral Presentation, not published

STRN NRL/JA/7330- 12- 1190
Route Sheet No. 7330/
Job Order No. 73- 4223- 01- 5
Classification   X _ U /UT   C
Sponsor   NASA
approval obtained ___ yes   X no

Title of Paper or Presentation
The Combined Effect of Reduced Spectral Bands and Increased Bandwidth on Shallow Water Remote Sensing: The Case of WorldView 2

Author(s) Name(s) (First,MI,Last), Code, Affiliation if not NRL

ZhongPing Lee Univ. of MA Boston Alan D. Weidemann 7333 Robert A Arnone 7330

It is intended to offer this paper to the _____
(Name of Conference)

_____
(Date, Place and Classification of Conference)

and/or for publication in **Transactions on Geoscience and Remote Sensing,** Unclassified
(Name and Classification of Publication)   (Name of Publisher)

After presentation or publication, pertinent publication/presentation data will be entered in the publications data base, in accordance with reference (a).
It is the opinion of the author that the subject paper (is ____) (is not ___X) classified, in accordance with reference (b).
This paper does not violate any disclosure of trade secrets or suggestions of outside individuals or concerns which have been communicated to the Laboratory in confidence. This paper (does ____) (does not ___X) contain any militarily critical technology.
This subject paper (has ____) (has never __X__) been incorporated in an official NRL Report.

Alan D. Weidemann, 7333
Name and Code (Principal Author)   (Signature)

CODE	SIGNATURE	DATE	COMMENTS
Author(s) Weideman		16/Apr/2012	Need by ___ 03 May 12
			Publicly accessible sources used for this publication
			This is a Final Security Review. Any changes made in the document after approved by Code 1226 nullify the Security Review.
Section Head N/A			
Branch Head Robert A Arnone, 7330		4/16/12	
Division Head Ruth H. Preller, 7300		4/16/12	1. Release of this paper is approved. 2. To the best knowledge of this Division, the subject matter of this paper (has ____) (has never __X__) been classified.
Security, Code 1231		4/19/12	1. Paper or abstract was released. 2. A copy is filed in this office.
Office of Counsel,Code 1008.3	Beede invention memo	4/24/2012	Sponsor Approval Attached.
ADOR/Director NCST E. R. Franchi, 7000			
Public Affairs (Unclassified/ Unlimited Only), Code 7030.4	Shannon Breland	4-23-12	approved
Division, Code			a final
Author, Code			

HQ-NRL 5511/6 (Rev. 12-98) (e)   THIS FORM CANCELS AND SUPERSEDES ALL PREVIOUS VERSIONS

Combined Effect of Reduced Band Number and Increased Bandwidth on Shallow Water Remote Sensing: The Case of WorldView 2

Zhongping Lee, Alan Weidemann, and Robert Arnone

Abstract—**WorldView 2 (WV2), launched in September 2009, is a satellite with hyperspatial resolution ($\sim$0.5–2 m) capability for Earth surface observation. It has eight spectral bands with enhanced signal-to-noise ratio to cover the visible-to-near-infrared (V–NIR) domain, thus providing a great potential for remote sensing of coastal ecosystem, in particular, the aquatic environments with shallow bottoms (e.g., coral reefs and seagrass beds). Traditionally, it requires $\sim$15 spectral bands in the V–NIR domain for reliable analytical retrieval of bottom properties (e.g., bathymetry) from remotely observed radiance spectrum. Data from WV2, however, have eight bands, and the width of each band is quite wide ($\sim$50 nm or more). Thus, the spectral configuration of WV2 is far from optimal for spectral remote sensing of various complex shallow environments, and it is important and necessary to know how such a band setting affects the reliability of remote-sensing retrievals. Here, we applied a hyperspectral optimization scheme [hyperspectral optimization processing exemplar (HOPE)] to a simulated shallow-bottom data set (sandy bottom) and compared retrievals from both hyperspectral and WV2 spectral settings. Retrieved results suggest that, for bottom contribution making up 40% or more of the measured signal, the depths derived from both hyperspectral and WV2 settings are generally consistent for waters shallower than 5 m. However, depths derived with WV2 setting have greater uncertainty and, in general, are shallower than those derived from the hyperspectral setting, particularly for waters deeper than 10 m. Options to produce higher confident properties from such band settings are discussed.**

Index Terms—**Bathymetry, coastal water, remote sensing.**

I. INTRODUCTION

THE high-spatial-resolution WorldView 2 (referred to as WV2 in the following text for brevity) satellite was launched in September 2009 (www.digitalglobe.com). Its Earth-observing sensor has eight spectral bands covering the visible-to-near-infrared (V–NIR) range. More interesting is the spatial resolution of the acquired image, which is $\sim$0.5–2 m making it possible to provide sharp observations of nearshore coastal environments where high spatial resolution is required

to distinguish changes of geophysical properties. Equipped with 11 bits of dynamic range, WV2 provides unprecedented radiometric measurements that can be used to provide highly desired geophysical properties of the land–ocean environments, and one of those products is the bathymetry of shallow coastal regions (www.digitalglobe.com). It has long been recognized that bathymetry of shallow bottom could be retrieved from measurement of water color [1]–[4], and successful retrievals of shallow water bathymetry from airborne [5]–[10] and satellite measurements [11], [12] have been presented in recent decades.

The retrieval of bottom properties requires high-quality radiometric measurements that can be adequately atmospherically corrected, as well as a sophisticated algorithm that can distinguish the various component contributions to the signal. The earlier methodologies to estimate bathymetry from water color generally take an empirical approach [1]–[4], where the empirical coefficients are image specific and thus are difficult to transfer from one image to another or between study areas. In addition, because the derivation of the coefficients requires *a priori* information, the application of this approach is difficult for inaccessible or difficult-to-reach areas. Other algorithm techniques [6], [13] use spectral optimization or lookup tables, which are based on radiative transfer and modeling of the bio-optical properties of the water column. These approaches relax the dependence of image-specific modification and are therefore more applicable to different regions. This study focuses on the spectral-optimization approach (SOA) for shallow water remote sensing.

In an earlier study, Lee and Carder [14] showed that the number of spectral bands positioned in the visible–infrared domain does impact the quality of retrieval of bottom properties. This is because, for the retrieval of bathymetry, it is important to maximize the measurable signal reflected back from the bottom. This return signal, however, depends on the spectral window of the water medium that is most transparent, which changes with water constituents. For a single sensor to cover most of the transparency windows of natural aquatic environments, Lee and Carder [14] suggested that a sensor should have at least $\sim$15 bands in the 400–800-nm spectral domain. WV2, however, has only seven bands in the $\sim$400–900-nm domain, and each band has a bandwidth of $\sim$50 nm. Fig. 1 shows an example of a hyperspectral remote-sensing reflectance spectrum (R_{rs}, in per steradian; ratio of water-leaving radiance to downwelling irradiance above the surface) with the corresponding spectral areas covered by the WV2 band settings. Many spectral features

Z. Lee is with the Department of Environmental, Earth, and Ocean Sciences, University of Massachusetts—Boston, Boston, MA 02125 USA (e-mail: zhongping.lee@umb.edu).

A. Weidemann and R. Arnone are with the Naval Research Laboratory, Stennis Space Center, MS 39529 USA (e-mail: alan.weidemann@nrlssc.navy.mil; bob.arnone@nrlssc.navy.mil).
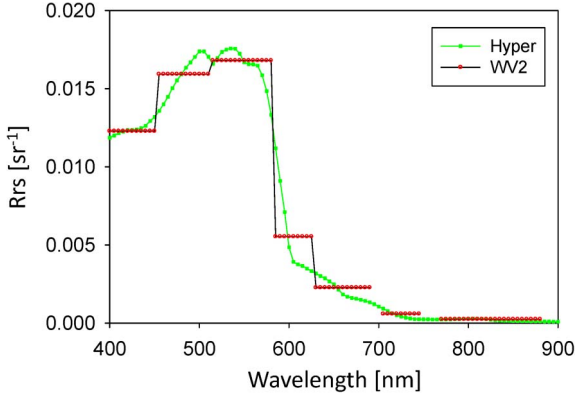
Fig. 1. Example of remote-sensing reflectance spectra represented by hyperspectral and WV2 band settings.

present in the hyperspectral data no longer exist in WV2 observations. Note that these spectral features play an important role in analytically retrieving subsurface geophysical information from remotely collected data [14], [15], and [31]. The measurement with limited wideband (LWB) setting, such as WV2, not only diminishes the spectral signature reflected from the bottom but also complicates the optical signals reflected back from the bottom and scattered by the water column. It is thus important to systematically evaluate and characterize the impacts of such LWB settings on the analytical retrieval of products such as shallow water bathymetry, since high-quality data products from WV2 are strongly desired for many applications.

II. DATA

It is not easy to visualize the combined impact of LWB settings on analytical retrievals. In order to characterize the impacts of LWB on remote-sensing retrievals, in particular, bathymetry, we use numerically simulated data of reflectance. In part, this is due to the shortage of concurrent measurements from both hyperspectral and WV2 sensors and comprehensive subsurface measurements.

To efficiently simulate wide range of spectral R_{rs} of optically shallow waters, we used an analytical model [13], [16] that describes R_{rs} as a function of properties of the bottom (depth and reflectance) and the water column (absorption and backscattering coefficients), instead of the widely used numerical model: Hydrolight [17]. However, this analytical expression was actually derived from Hydrolight simulations [13], [16], and R_{rs} modeled using the analytical expression agrees with that from the more precise numerical simulation within $\pm 10\%$.

Following Lee *et al.* [13], above-surface remote-sensing reflectance can be expressed as

$$
\begin{aligned}
R_{rs} &= G\, r_{rs} \\
r_{rs} &= r_{rs}^C + r_{rs}^B \\
&= r_{rs}^{dp}\left(1 - e^{-D_c(a+b_b)H}\right) + \frac{\rho}{\pi} e^{-D_B(a+b_b)H}.
\end{aligned} \tag{1}
$$

r_{rs} (in per steradian) is the subsurface remote-sensing reflectance, and parameter G accounts for the cross-surface impact that includes sea-to-air transmission as well as subsurface internal reflection [16], [18], [19]. Terms r_{rs}^C and r_{rs}^B represent the contribution from water column and the bottom,

respectively. In addition, r_{rs}^{dp} is the subsurface remote-sensing reflectance when the bottom is optically deep (i.e., bottom effects to r_{rs} are negligible) and is expressed as [20]

$$
r_{rs}^{dp} = g_w \frac{b_{bw}}{a + b_b} + g_p \frac{b_{bp}}{a + b_b}. \tag{2}
$$

g_w is taken as 0.113 sr^{-1}, while g_p is modeled as

$$
g_p = 0.197 \left(1 - 0.636\, e^{-2.552 \frac{b_{bp}}{a + b_b}}\right). \tag{3}
$$

$D_{C,B}$ are model parameters that account for the elongation of photon path lengths in the water due to scattering. The a and b_b are the absorption and backscattering coefficients (in per meter), respectively, with ρ as the bottom reflectance and H as the bottom depth (in meters). Except for H, all other variables are functions of wavelength (λ, in nanometers; omitted here for brevity). Note that values of ρ, H, a, and b_b are required for the generation of R_{rs}. The spectral absorption and backscattering coefficients are described by [19]

$$
\begin{aligned}
a(\lambda) &= a_w(\lambda) + a_{ph}(\lambda) + a_{dg}(\lambda) \\
b_b(\lambda) &= b_{bw}(\lambda) + b_{bp}(\lambda)
\end{aligned} \tag{4}
$$

where $a_w(\lambda)$ and $b_{bw}(\lambda)$ are the absorption and backscattering coefficients of pure water, respectively, and their values are known [21], [22], and $a_{ph}(\lambda)$, $a_{dg}(\lambda)$, and $b_{bp}(\lambda)$ are the absorption and backscattering coefficients of phytoplankton, detritus–gelbstoff, and particulates, respectively, with values taken from the International Ocean Colour Coordinating Group (IOCCG) database [23]. It is important to recognize that the spectral shapes of the three inherent optical properties $[a_{ph}(\lambda), a_{dg}(\lambda),$ and $b_{bp}(\lambda)]$ of this database are not constant, and the shapes of $a_{ph}(\lambda)$ were taken from field measurements. The IOCCG database is extensive and has 500 data sets covering clearer to turbid waters and therefore can be assumed to be representative of many coastal and open-ocean conditions. We took the first 300 only ($a(440)$ in a range of $\sim 0.015-0.4$ m^{-1}) for the studies here, as it is less likely to detect the bottom in turbid waters. In addition, because the spectral resolution of the IOCCG data is 10 nm, we interpolated the spectra of $a_{ph}(\lambda)$, $a_{dg}(\lambda)$, and $b_{bp}(\lambda)$ to every 5 nm in order to generate "hyperspectral" R_{rs}. Furthermore, the spectral range of the IOCCG data set is 400–800 nm, which is further extended to 900 nm to cover the longer band of WV2. Specifically, (4) was used for this expansion. For the 800–900-nm spectral window, $a_w(\lambda)$ values were taken from Hale and Querry [24]; $a_{ph}(\lambda)$ was taken as the value of $a_{ph}(800)$; $a_{dg}(\lambda)$ was extended from $a_{dg}(800)$ with an exponential function of wavelength where the spectral slope was provided in the IOCCG data set; and $b_{bp}(\lambda)$ was extended from $b_{bp}(800)$ with a power function of wavelength where the power coefficient was also provided in the IOCCG data set.

Eleven values of H were selected: 0.3, 0.5, 0.9, 1.5, 2.6, 4.5, 8, 12, 15, 19, and 25, representing roughly an increase rate of 60% and a maximum retrievable depth of 25 m for the modeling effort. Further, although different substrates have different bottom reflectivities, a single and spectrally constant

bottom reflectance was designated here. The reason for this is threefold: 1) Our focus here is to compare and contrast remote-sensing retrievals between hyperspectral and LWB settings; 2) even though only one bottom reflectance was employed, bottom depth and water-column optical properties were not constant and the latter varies spectrally; the combined effect of bottom contribution to the above-surface remote-sensing reflectance (that a remote sensor measures) is equivalent to that of using various bottom reflectances; and 3) in remote-sensing inversion, a different spectral shape for bottom reflectance was used (see Section III), which avoided circular calculation and is consistent with real-world situation (i.e., the spectral information of the bottom has to be estimated or assumed). A bottom albedo of 0.2 and assumed spectrally flat was used for all the combination of water and depth values. Thus, 3300 sets of $R_{rs}(\lambda)$ were generated through the combinations of the 11 H values and the 300 a and b_b spectra. Maximum contribution from the bottom is calculated as

$$M_B = \max\left(\frac{r_{rs}^B(\lambda)}{r_{rs}(\lambda)}\right). \tag{5}$$

Of this data set, there are ~85% that have M_B greater than 0.2 (20% of the total spectral signal) and ~72% that have M_B greater than 0.5.

After the generation of the 3300 sets of hyperspectral R_{rs}, equivalent R_{rs}'s at WV2 bands were calculated with the following approximation:

$$R_{rs}^{LWB}(B_i) \approx \frac{\int_{400}^{900} R_{rs}(\lambda)F_{Bi}^{LWB}(\lambda)d\lambda}{\int_{400}^{900} F_{Bi}^{LWB}(\lambda)d\lambda} \tag{6}$$

with $F_{Bi}^{LWB}(\lambda)$ as the band response function of Band #i. For the study here, a boxcar function was assumed for each band with the bandwidth of each band the same as those of WV2.

III. INVERSION OF BOTTOM AND WATER PROPERTIES VIA SPECTRAL OPTIMIZATION

A. HOPE for Hyperspectral Data

We applied the hyperspectral optimization processing exemplar (HOPE) technique and protocols [5], [7], [11], [13] to retrieve bottom and water properties of the 3300 hyperspectral and WV2 data sets and then compared the retrievals with known properties to characterize the impacts of LWB. HOPE basically uses the spectral matching concept to derive subsurface properties of interest, and the following briefly summarizes the models used in HOPE and the optimization procedure.

In general, we used the same analytical structure to link remote-sensing reflectance with subsurface properties. Because the 3300 data sets are numerically simulated, we used different r_{rs}^{dp} and bio-optical models for the inherent optical property (IOP) components in the inversion process to avoid circular calculation. Specifically, r_{rs}^{dp} takes the form as that in Gordon *et al.* [18]

$$r_{rs}^{dp} = \left(g_0 + g_1 \frac{b_b}{a + b_b}\right)\frac{b_b}{a + b_b} \tag{7}$$
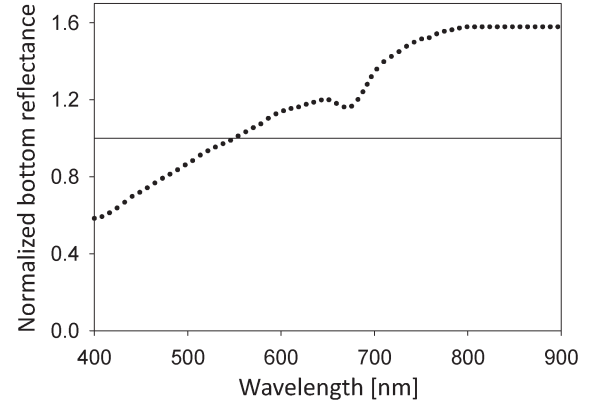

Fig. 2. Spectral shape of bottom reflectance. Dotted spectrum is used in the optimization inversion; solid curve is used in the data simulation.

with values of g_0 and g_1 taken as 0.089 and 0.125 sr^{-1} [25], respectively.

Further, the three IOP spectra are modeled as

$$a_{ph}(\lambda) = [a_0(\lambda) + a_1(\lambda)\ln(P)]P$$
$$a_{dg}(\lambda) = G\exp(-S(\lambda - 440))$$
$$b_{bp}(\lambda) = X\left(\frac{440}{\lambda}\right)^Y \tag{8}$$

where values for $a_0(\lambda)$ and $a_1(\lambda)$ are known [16] and Y is estimated for each R_{rs} spectrum [25] with S taken as 0.015 nm^{-1} for default. P and G represent the absorption coefficient of phytoplankton and detritus–gelbstoff, and X represents the backscattering coefficient of particles, all at 440 nm. These IOP spectra are completely independent of the spectra used for the generation of the simulated data sets.

The spectrum of bottom reflectance was modeled as

$$\rho(\lambda) = \boldsymbol{B}\rho_{bot}^+. \tag{9}$$

Here, ρ_{bot}^+ is the 550-nm normalized bottom spectral reflectance, and to be different from the input bottom reflectance, a sandy bottom spectrum [5] (see Fig. 2), which generally increases with wavelength, was used. B value here thus represents retrieved bottom reflectance at 550 nm.

After these modeling considerations, each spectral R_{rs} can then be expressed as

$$R_{rs}(\lambda_1) = F(a_w(\lambda_1), b_{bw}(\lambda_1), \boldsymbol{P}, \boldsymbol{G}, \boldsymbol{X}, \boldsymbol{B}, \boldsymbol{H})$$
$$R_{rs}(\lambda_2) = F(a_w(\lambda_2), b_{bw}(\lambda_2), \boldsymbol{P}, \boldsymbol{G}, \boldsymbol{X}, \boldsymbol{B}, \boldsymbol{H})$$
$$\vdots$$
$$R_{rs}(\lambda_n) = F(a_w(\lambda_n), b_{bw}(\lambda_n), \boldsymbol{P}, \boldsymbol{G}, \boldsymbol{X}, \boldsymbol{B}, \boldsymbol{H}). \tag{10}$$

Therefore, there are just five unknowns to model a spectral R_{rs}, and HOPE numerically solves for the five unknowns in (10) via spectral optimization, i.e., to minimize an objective function (11) that quantitatively compares modeled (10) and measured

(the numerically simulated here) spectral R_{rs}. The objective function was updated as

$$\text{err}_{\text{Rrs}} = \frac{\sqrt{\Lambda_{\lambda_1}^{\lambda_2}\left(R_{rs}(\lambda)-\widetilde{R}_{rs}(\lambda)\right)^2 + w\,\Lambda_{\lambda_3}^{\lambda_4}\left(R_{rs}(\lambda)-\widetilde{R}_{rs}(\lambda)\right)^2}}{\Lambda_{\lambda_1}^{\lambda_2}\left(R_{rs}(\lambda)\right)+w\,\Lambda_{\lambda_3}^{\lambda_4}\left(R_{rs}(\lambda)\right)} \tag{11}$$

with $\widetilde{R}_{rs}$ for values from (10) and R_{rs} for values from measurements. In (11), $\Lambda_{\lambda_1}^{\lambda_2}$ represents an average of the array $[R_{rs}(\lambda)]$ defined by the range of wavelengths, with $\lambda_1-\lambda_2$ and $\lambda_3-\lambda_4$ for the blue–yellow range (400–650 nm) and yellow–red/infrared (650–900 nm) range, respectively. The err_{Rrs} thus provides a quantitative measure of the relative difference between modeled and measured spectral R_{rs}'s. This objective function differs slightly from the earlier practices by introducing a weighting factor (w), which is defined as

$$w = \frac{\Lambda_{\lambda_1}^{\lambda_2}\left(R_{rs}(\lambda)\right)}{\Lambda_{\lambda_3}^{\lambda_4}\left(R_{rs}(\lambda)\right)}. \tag{12}$$

This was included because, for most shallow waters, the transparency window is in the blue–green domain, and therefore, R_{rs} in this spectral window could be significantly larger than the R_{rs} in the yellow–red window. Consequently, err_{Rrs} could be dominated by the R_{rs} difference in the blue–green window in the traditionally defined err_{Rrs} function [13]. In other words, without this weighting factor, err_{Rrs} is dominated by the variations in the $\lambda_1-\lambda_2$ window, which then could limit the search of results that provide optimal matches in the $\lambda_3-\lambda_4$ range. With the introduction of w, a balanced evaluation across the shorter and longer wavelengths is better achieved. For data with high noise in the longer wavelengths, however, it is either required to smooth the image in those bands or skip the use of this weighting factor; otherwise, the noise would be magnified.

In the HOPE process, values of P, G, X, B, and H are initiated pixelwise (e.g., Lee *et al.* [5]) and here are taken as

$$\begin{aligned} P &= 0.05\left(\frac{R_{rs}(440)}{R_{rs}(550)}\right)^{-1.7} \\ G &= 1.5\,P \\ X &= 0.1\,P \\ B &= 0.1 \\ H &= 0.3. \end{aligned} \tag{13}$$

To generate physically meaningful solutions, boundaries of the five variables are required. For this investigation, a range found in typical coastal waters is used

$$0.002 \le P \le 0.7 \text{ m}^{-1}$$
$$0.001 \le G \le 3.5 \text{ m}^{-1}$$
$$0.0002 \le X \le 0.1 \text{ m}^{-1}$$
$$0.01 \le B \le 0.9$$
$$0.02 \le H \le 35 \text{ m}.$$

To derive the five variables for each R_{rs}, we used the Solver tool included in MS Excel. This tool uses several algorithms to find optimal solutions that include the generalized reduced gradient nonlinear solving method developed by Lasdon *et al.* [26] and the simplex LP solving method implemented by Fylstra *et al.* [27].

B. Optimization Scheme for LWB Setting

For the WV2 sensor or any other LWB sensor, R_{rs} is measured at a specific band, not at a specific wavelength. Therefore, the objective function is written as (14) and (15), shown at the bottom of the page. B_i represents the ith band of the sensor, and only the first seven bands were used. The eighth band, which is centered at 949 nm, has nearly no information of the water or the bottom. In the optimization process, $\widetilde{R}_{rs}(B_i)$ is the modeled R_{rs} at Band i and is calculated with the following steps: 1) Hyperspectral (400–900 nm; 5-nm resolution) R_{rs} is generated using the five variables (10), and 2) the hyperspectral R_{rs} is convolved to WV2 R_{rs} using (6).

IV. Results and Discussion

Before we compare the retrieved bathymetry and absorption values, Fig. 3 shows the err_{Rrs} values of the 3300 points, for both the hyperspectral and LWB optimizations. These values are generally under 0.035 (or 3.5%), and as expected, err_{Rrs} values of WV2 are smaller than that of the hyperspectral solution. The err_{Rrs} values in the figure basically provide a confidence check about the SOA scheme and indicate that the output values of this study were indeed those when err_{Rrs} was minimized under the designed optimization system. It is necessary to point out that, because SOA, in general, is an implicit numerical solution process, a smaller err_{Rrs} value does not necessarily indicate higher quality retrievals (sometimes, negative parameters achieves even smaller err_{Rrs}, for instance).

$$\text{err}_{\text{Rrs}}^{\text{WV2}} = \sqrt{\frac{\Lambda_{B_1}^{B_4}\left(R_{rs}(B_i)-\widetilde{R}_{rs}(B_i)\right)^2 + w\,\Lambda_{B_5}^{B_7}\left(R_{rs}(B_i)-\widetilde{R}_{rs}(B_i)\right)^2}{\Lambda_{B_1}^{B_4}\left(R_{rs}(B_i)\right)+w\,\Lambda_{B_5}^{B_7}\left(R_{rs}(B_i)\right)}} \tag{14}$$

$$w = \frac{\Lambda_{B_1}^{B_4}\left(R_{rs}(B_i)\right)}{\Lambda_{B_5}^{B_7}\left(R_{rs}(B_i)\right)} \tag{15}$$
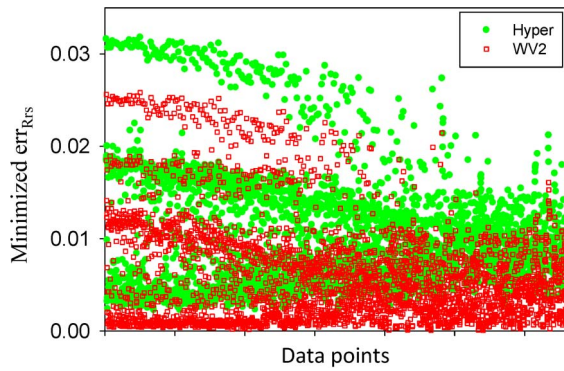
Fig. 3. Range of minimized err_{Rrs} of this study. Left to right represents sequential order of the 3300 data sets.
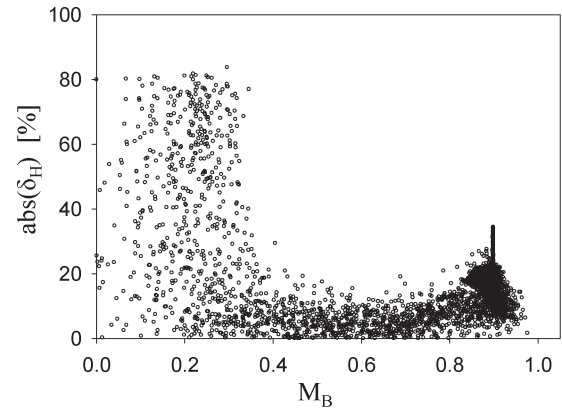

Fig. 4. Scatter plot between M_B and $\text{abs}(\delta_H)$ of the 3300 data sets, which shows a general trend of smaller $\text{abs}(\delta_H)$ with higher M_B.

On the other hand, erroneous retrievals will be derived if the optimization process stopped prematurely.

To quantitatively measure the difference between retrieved and known values, the signed percent difference for each data point was calculated as

$$\delta_Q = \left(\frac{Q_{\text{der}}}{Q} - 1 \right) \times 100 \qquad (16)$$

with Q representing a known value (input value) and Q_{der} representing SOA-derived value.

As anticipated, the retrieval of bottom (or water column) properties strongly depends on the bottom (or water column) signal contribution to the $R_{\text{rs}}(\lambda)$ spectrum. As an example, Fig. 4 shows the relationship between M_B and the absolute value of δ_H, $\text{abs}(\delta_{H-\text{hyper}})$, with H derived from hyperspectral setting. Not surprisingly, when M_B decreases, $\text{abs}(\delta_{H-\text{hyper}})$ increases, particularly for $M_B < \sim 0.4$. However, as M_B approaches 1.0, $\text{abs}(\delta_{H-\text{hyper}})$ gets slightly larger. This is because of the mismatch of the spectral shape of bottom reflectance (see Fig. 2). When M_B is getting closer to 1.0, most of $R_{\text{rs}}(\lambda)$ comes from the bottom, and this information is presented almost in the entire V–NIR spectrum. Consequently, the use of a proper bottom spectral shape is important for the retrieval of bottom properties. For intermediate M_B values (for example, $M_B = 0.5$), the transparent window (for instance, around 570 nm for coastal areas) contains most of the bottom information, while the bottom signal in the shorter and longer wavelengths are diminished due to water's attenuation (water itself and the presence of plankton and dissolved materials). Consequently, the match of the entire spectral shape of bottom reflectance is no longer that important, and lower $\text{abs}(\delta_{H-\text{hyper}})$ is achieved. In short, if the bottom reflectance has strong spectral signature in the transparent window (which could be narrow or wide), it is always important to have a matching spectral albedo shape in this window for better retrieval of bottom properties.

The aforementioned results indicate that, for high-quality retrieval of bottom properties (depth), it is, in general, sufficient to use a value of about 0.4 for M_B as an effective criterion. Thus, in the following, we focus on the results where M_B is greater than 0.4.

A. M_B Known From Input

To characterize the retrieval of the SOA, Figs. 5(a) and (b) compares retrieved H with known depth for bottoms with $M_B \geq 0.4$, and M_B was calculated using simulated remote-sensing information (2533 data points). For a depth range of 0.3–25 m with wide variation of water properties, the coefficient of determination (R^2), the slope, and the bias are 0.996, 1.03, and 0.17, respectively, for the hyperspectral retrieval, and they are 0.985, 0.973, and 0.31, respectively, for the WV2 retrieval. For the percent difference, $\delta_{H-\text{hyper}}$ is in a range of -17.5% to 34.4%, while $\delta_{H-\text{WV2}}$ is in a range of -42.4% to 37.6%. As shown here and in previous studies [6], [7], [11], generally, the retrieved depths match known depths very well when hyperspectral measurements are available. This is in part due to the strong bottom signal in R_{rs} spectra. However, when hyperspectral signal is degraded to LWB settings, the range of error of retrieved H is increased by $\sim50\%$ even for $M_B \geq 0.4$.

To further highlight the impact of LWB on shallow depth retrieval, Fig. 5(c) compares the WV2-retrieved depth with the hyperspectrally retrieved depth for $M_B \geq 0.4$. The δ_H between WV2 retrieval and hyperspectral retrieval is in a range of -48.2% to 26.6%. Statistically, the two retrievals are quite consistent ($R^2 = 0.987$, slope = 0.94, and bias = 0.15). The smaller than 1.0 slope and the small bias indicate that H_{WV2} tends to predict shallower depths than H_{hyper} for this data set. It is interesting to note that most of the difference appeared for $H > \sim 10$ m. Because SOA solves for five variables simultaneously with a simple objective of obtaining the smallest err_{Rrs}, it is not easy to visualize the cause and effect associated with the LWB setting. Generally, the increasing difference between hyperspectral and WV2 retrievals may stem from at least three reasons. First, with a greater depth and a larger absorption in the blue bands, the R_{rs} spectrum will have a sharper peak around blue–green transparent window (see Fig. 1 for an example). Hyperspectral measurements will be able to observe this peak, but measurements with LWB settings will not only miss the peak but also level the spectrum in various degrees (see the red line in Fig. 1). Second, because of this leveling of the spectrum, the red edge (> 600 nm) measured by WV2
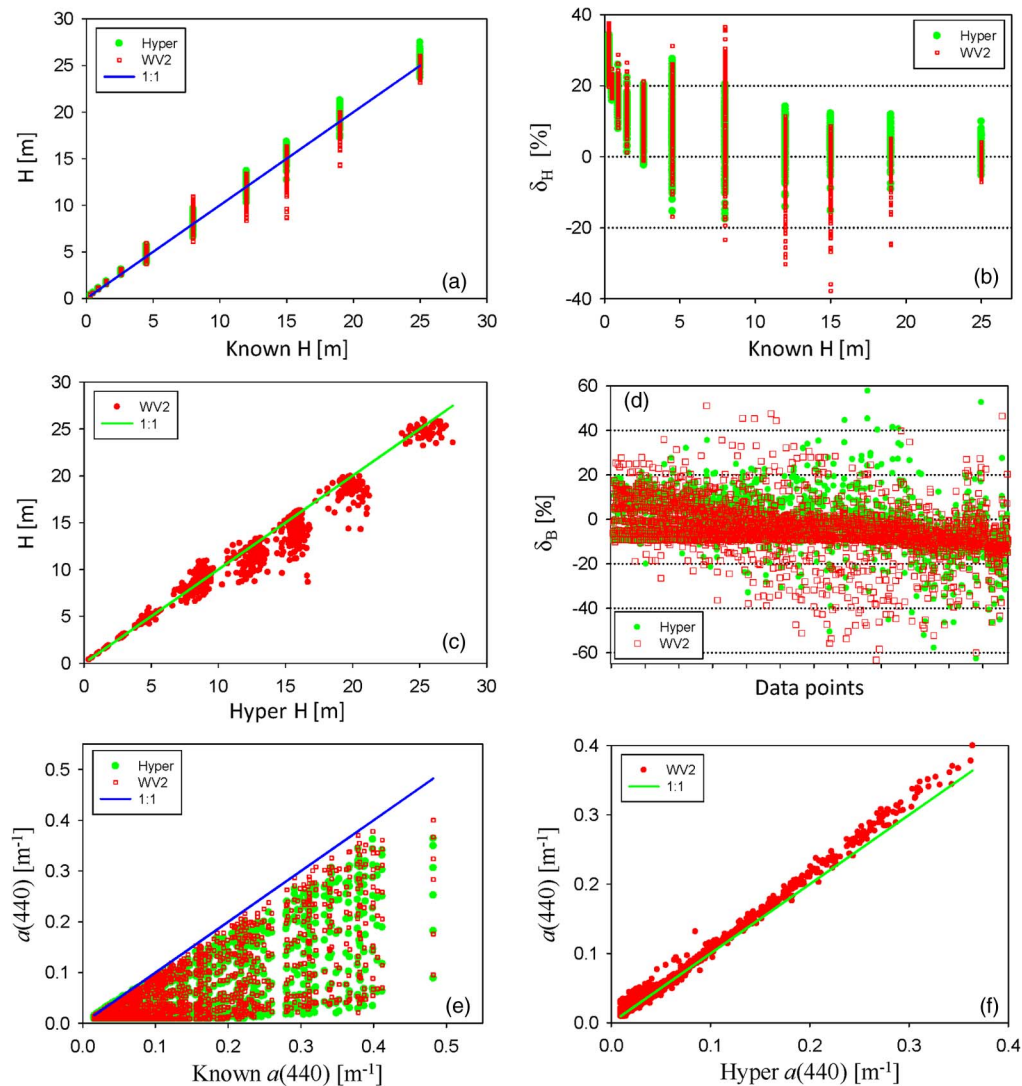
Fig. 5. Retrieval results of known $M_B \geq 0.4$, for both hyperspectral and WV2 band settings. (a) Scatter plot between derived and known depths. (b) Variation of δ_H and its relationship with known depth. (c) Scatter plot between WV2-retrieved and hyperspectrally retrieved depths. (d) Range of δ_B. As in Fig. 3, X-axis represents sequential order of the 3300 data sets. (e) Scatter plot between derived and known absorption coefficients at 440 nm. (f) Scatter plot between WV2-retrieved and hyperspectrally retrieved absorption coefficients at 440 nm.

will be higher than that measured by a hyperspectral sensor for the same corresponding region. And, third, the absorption coefficients in the longer wavelengths are nearly constant due to the strong contribution of water absorption itself; therefore, the simplest solution by the optimization code is to use a smaller H value in order to get larger R_{rs} value in order to match the elevated WV2 values. As a consequence, the shorter wavelengths will then be compensated by adjustments to the absorption coefficients, where there are two independent variables (P and G). Also, note that, here, the bottom reflectance used in the inversion has higher relative contribution in the red than in the blue–green compared to the bottom reflectance used in the simulation. If it is a reversed situation, i.e., simulation with a sandy bottom spectral shape but inversion with a spectrally flat spectral shape, an even shallower H might be necessary in order to compensate the reduced relative contribution of the bottom in the longer wavelengths for high M_B cases. In short, because of the various combinations of water and bottom properties and the complexity of an SOA system, we cannot draw a

general conclusion that, each time, H_{WV2} will be shallower than H_{hyper} [as shown in Fig. 5(c)].

For bottom reflectance at 550 nm, the percentage difference is generally within $\pm 20\%$ [see Fig. 5(d)], which indicates that, when $M_B \geq 0.4$, it is quite confident to retrieve a reliable bottom property at 550 nm, at least for the sandy bottom case. However, this does not mean that we will retrieve similar quality of bottom reflectance values at other wavelengths. Fundamentally, in the current SOA scheme, bottom reflectances at other wavelengths are not derived independently from R_{rs} measured at those wavelengths but inferred with a predefined bottom spectral shape [see (9)]. Therefore, for the simulated data sets where the input spectrum is spectrally flat while the output spectrum is spectrally reddish, less accurate results will occur for other wavelengths (underestimation at shorter wavelengths and overestimation at longer wavelengths for this data set) even if we have perfect results at 550 nm. The impact of this error (or uncertainty) is propagated to water properties (as discussed later).
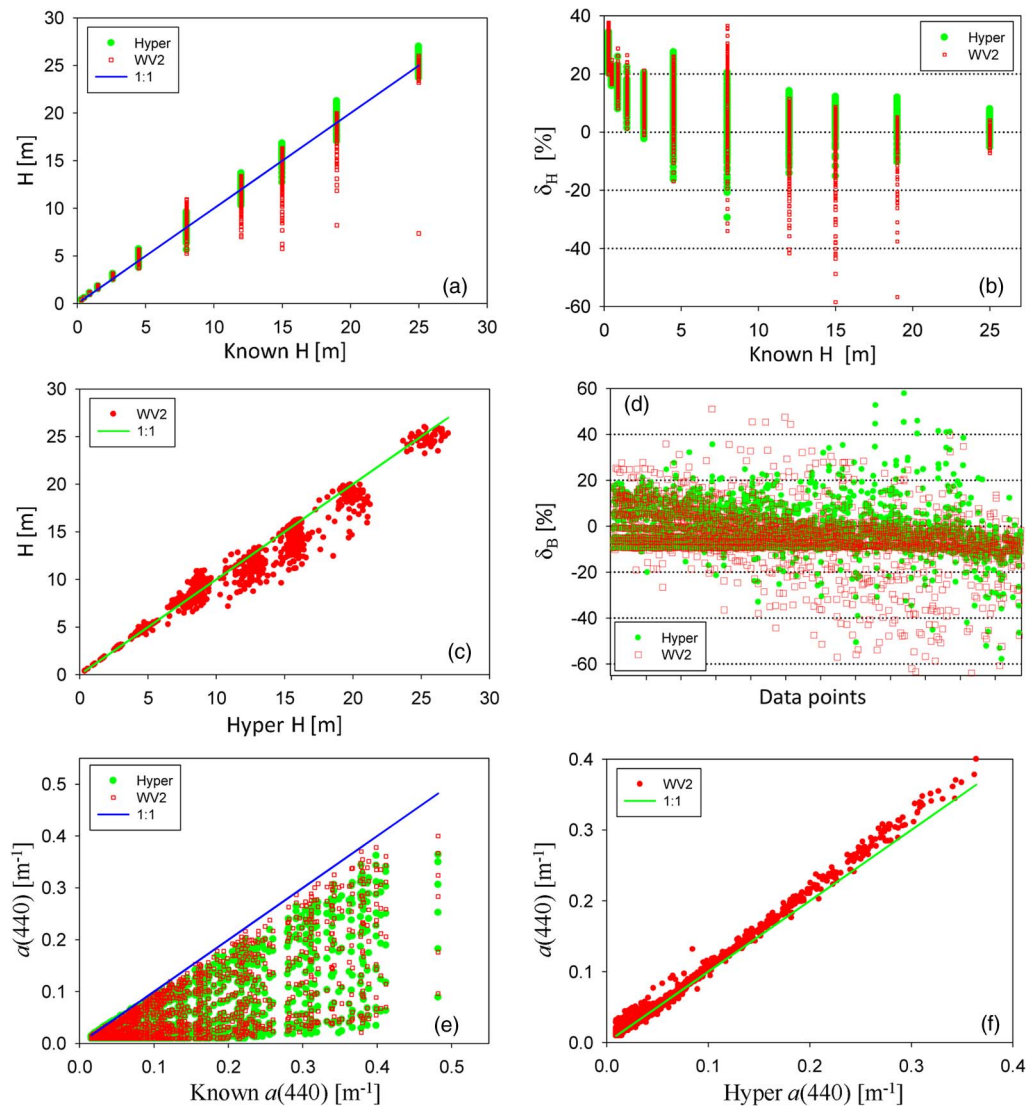
Fig. 6.   As in Fig. 5 for retrievals of $M_B \geq 0.4$, but M_B is calculated from derived R_{rs} information when the optimization is reached.

The retrieved absorption coefficients at 440 nm from both hyperspectral and WV2 settings do not match well with known values when $M_B \geq 0.4$ [see Fig. 5(e)]. This is because, when the M_B value is large, there is less contribution to the total R_{rs} from the water column. Consequently, a larger uncertainty is expected in retrieving water properties. The systematic lower $a(440)$, however, is due to the spectral shape of bottom reflectance used in the retrieval which is red rich compared to the spectral shape used for the data simulation (see Fig. 2). To compensate for the smaller bottom reflectance in the shorter wavelengths, a smaller total absorption coefficient is required (where there are two free variables) in order to achieve a good match between known and derived R_{rs}'s. Similarly, if the simulation is with a sandy bottom spectral shape (see Fig. 2) while the inversion is with a spectrally flat spectral shape, a higher absorption coefficient will be expected as it is required to compensate for the elevated bottom contribution from the shorter wavelengths. These results indicate that, for an aquatic environment with a shallow bottom, the quality of retrieved water or bottom properties is highly dependent on their relative contributions in the measured R_{rs} and the close-

ness of the spectral shape used in the inversion versus the actual environment.

B. M_B Derived From R_{rs}

For a remote-sensing scenario, the only available information is R_{rs} along with auxiliary data (such as time and location), the M_B value is not known *a priori*, and this value must be derived from the measured R_{rs}. The following uses modeled R_{rs} when the optimization is reached to calculate M_B and evaluate the SOA results. We again focus on retrievals with $M_B \geq 0.4$ to characterize the effects of LWB, with results shown in Fig. 6. With such a criterion, depth retrieved with the hyperspectral setting still compared very well with known values ($R^2 = 0.995$, slope $= 1.03$, and bias $= 0.17$), and δ_H is in a range of -29.4% to 34.4%. The number of points with $M_B \geq 0.4$, however, became 2582 (as compared with 2533 mentioned earlier), which indicates that a few deeper bottoms were falsely interpreted as optically shallow bottoms.

When M_B was derived with the WV2 band setting, the number of points with $M_B \geq 0.4$ became 2598, i.e., even
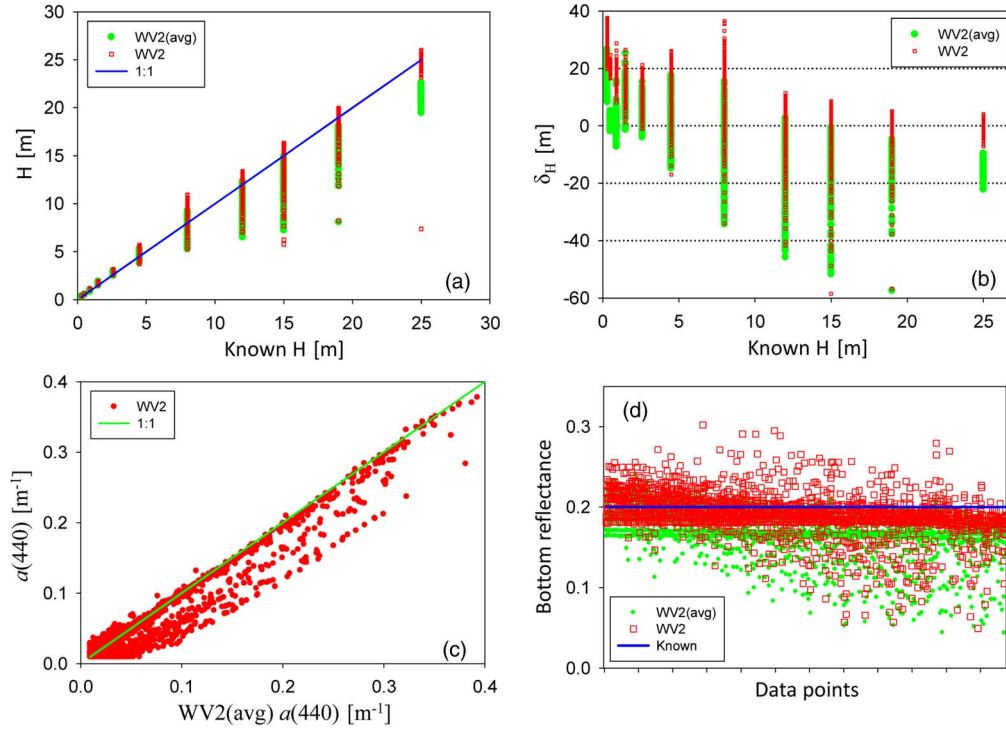
Fig. 7. Comparison between the results of WV2 band settings, one using band-averaged modeling coefficients [represented as WV2(avg)] and the other using hyperspectral modeling coefficients then convolved to WV2 bands. (a) Scatter plot between derived and known depths. (b) Variation of δ_H and its relationship with known depth. (c) Scatter plot between WV2- and WV2(avg)-retrieved $a(440)$. (d) Range of WV2- and WV2(avg)-retrieved bottom reflectances at 550 nm.

more points falsely categorized into optically shallower bottom. Furthermore, compared to known depths, δ_H is in a range of -70.6 to 37.6% ($R^2 = 0.972$, slope $= 0.95$, and bias $= 0.35$). These results clearly indicate that larger uncertainties resulted from the LWB setting, particularly more points being falsely classified as shallower bottoms. Compared to H_{hyper}, H_{WV2} is generally shallower, and again, most of these occurred for $H_{\mathrm{hyper}} > \sim 10$ m. For depth less than 5 m, retrievals from both hyperspectral and WV2 settings are about the same, as long as $M_B \geq 0.4$. To improve the confidence of depth retrieval from the WV2 band setting, particularly for deeper bottoms, it is necessary to have a more stringent criterion about optically shallow bottoms. For example, if we set $M_B \geq 0.6$, the range of δ_H became -28.4% to 37.6%.

Because of the retrieval of false optically shallow water, the bottom reflectance at 550 nm derived with the WV2 setting is slightly worse (average of $\mathrm{abs}(\delta_B) = 10.7\%$) than that derived with the hyperspectral setting (average of $\mathrm{abs}(\delta_B) = 9.4\%$). The results of water's absorption coefficient are similar to those retrieves when M_B is calculated from known R_{rs} information, i.e., retrieved values are significantly smaller than known values. In addition, $a(440)$ from the WV2 setting is slightly higher than that obtained with the hyperspectral setting, again, a consequence of slightly shallower H value.

C. Results With Band-Averaged Model Coefficients

For data sets measured by LWB sensors, another common practice in analytical remote sensing is to model the measured R_{rs} of each band with band-averaged coefficients; then, (10) can be written as

$$R_{\mathrm{rs}}(B_1) = F\left(a_w(B_1), b_{\mathrm{bw}}(B_1), \boldsymbol{P}, \boldsymbol{G}, \boldsymbol{X}, \boldsymbol{B}, \boldsymbol{H}\right)$$
$$R_{\mathrm{rs}}(B_2) = F\left(a_w(B_2), b_{\mathrm{bw}}(B_2), \boldsymbol{P}, \boldsymbol{G}, \boldsymbol{X}, \boldsymbol{B}, \boldsymbol{H}\right)$$
$$\vdots$$
$$R_{\mathrm{rs}}(B_n) = F\left(a_w(B_n), b_{\mathrm{bw}}(B_n), \boldsymbol{P}, \boldsymbol{G}, \boldsymbol{X}, \boldsymbol{B}, \boldsymbol{H}\right) \quad (17)$$

i.e., all constants to model R_{rs} (like a_w and b_{bw} and model coefficients for phytoplankton absorption coefficient, for example) are taken as band-averaged values. Compared to (10), the aforementioned equation also consists of five variables, and they can be retrieved with the same objective function (14) and the same optimization tool.

For the 3300 simulated WV2 spectra, we retrieved bottom and water-column properties and compared the results with known values and those retrieved using the hyperspectral model convolved approach (Section III-B), with the results shown in Fig. 7. Generally, both approaches generated quite consistent results (except one point of significant underestimation of H by the spectral-convolved scheme). With the band-averaged model coefficients, for $M_B \geq 0.4$ (2576 points, calculated from modeled $R_{\mathrm{rs}}(B_i)$ when optimization is reached), δ_H is in a range of -57.4% to 26.7% ($R^2 = 0.968$, slope $= 0.82$, and bias $= 0.33$) when compared with the known depth. These results are similar to that using hyperspectral-convolved LWB, but H retrieved with the band-averaged coefficients is generally underestimated by $\sim 15\%$, particularly for $H > \sim 5$ m.

This is because an LWB sensor measures total effect and the relationship between R_{rs} and a, b_b, and H is not linear [28]. Thus, (17) is not exactly accurate between band-averaged R_{rs} and band-averaged a and b_b. This average should be spectrally weighted by the relative contribution of water and bottom properties. Because water and bottom properties change significantly from location to location, one set of band-averaged values will not work for all cases (i.e., no universal values). The better results for $H < 5$ m are because, for the data set used, these cases generally have $M_B \geq \sim 0.8$, and therefore, the modeling of water properties is no longer that important since most of the signal in the measured R_{rs} comes from the bottom contribution.

Further, because of using the band-averaged coefficients, the retrieved B (bottom reflectance at 550 nm) values with the band-averaged scheme are generally lower than the known values (average of abs(δ_B) $\sim 16\%$). Note that it is $\sim 10\%$ for the spectral-convolved scheme. This is because of the smaller H (shallower depths); subsequently, the exponential function related to the bottom contribution will be larger, and a smaller B value is necessary to compensate this enhancement. Another effect of the shallower depth is the slightly larger total absorption coefficient when using the band-averaged scheme.

From the aforementioned comparison, it suggests that it is better to use a hyperspectral-convolved approach for analytical remote sensing of LWB measurements, particularly for depths deeper than ~ 5 m. If an approach with band-averaged coefficients is necessary, such coefficients should not be simple arithmetic averages of the hyperspectral constants (like a_w, b_{bw}, etc.) based on the band-response function but rather an optimized set of coefficients based on wide combinations of water and bottom properties.

V. SUMMARY

With a wide dynamic data set and using an analytical hyperspectral inversion algorithm, it has been found that if the bottom contribution makes up 40% or more of the total measured radiance, retrieval of bottom depth with the WV2 band setting has equivalent fidelity to that obtained using a hyperspectral setting, particularly if the bottom depth is within 5 m (or bottom contribution makes 80% or more of the total signal). Larger uncertainties with the WV2 band setting are found for deeper bottom depths, which require a more stringent criterion about the bottom contribution (e.g., 60% from bottom) in order to enhance the fidelity of remotely retrieved depth for the WV2 sensor. Results from this study also indicate that, for such wideband measurements, because R_{rs} is not a linear function of either the water or bottom properties, it is better to use a hyperspectral model accompanied with spectral convolution to model the band-averaged R_{rs} instead of using band-averaged modeling coefficients to model the band-averaged R_{rs}. Although the study here used a sandlike bottom and used WV2 band setting as an example, the conclusions should also be applicable to other bottom substrates or other LWB sensors (e.g., System for Earth Observation, IKONOS, etc.), i.e., LWB setting will affect bottom retrievals, but the extent will depend on the relative contribution of bottom to the total signal and the ability to match the bottom spectral shape used in inversion versus the actual bottom substrate when the bottom is quite shallow optically.

It is necessary to point out that the aforementioned conclusions apply only to analytical inversion schemes. For empirical approaches (e.g., Lee *et al.* [29] and Loomis [30]), such band-setting effects will be included in the empirically derived transfer coefficients, although they could be image or region specific. Another challenge for remote sensing with LWB sensor types is the atmosphere correction, as specific bands will also extend over the various gas spectral absorption regions and includes their effects. High-quality atmospheric correction of LWB sensors is critical before any analytical algorithms can be applied to retrieve subsurface properties and, as such, is an area that demands further effort.

REFERENCES

[1] F. C. Polcyn, W. L. Brown, and I. J. Sattinger, *The Measurement of Water Depth by Remote-Sensing Techniques*. Ann Arbor, MI: Univ. Michigan, 1970.

[2] R. K. Clark, T. H. Fay, and C. L. Walker, "Bathymetry calculations with Landsat 4 TM imagery under a generalized ratio assumption," *Appl. Opt.*, vol. 26, no. 19, pp. 4036–4038, Oct. 1987.

[3] D. R. Lyzenga, "Remote sensing of bottom reflectance and water attenuation parameters in shallow water using aircraft and Landsat data," *Int. J. Remote Sens.*, vol. 2, no. 1, pp. 71–82, 1981.

[4] W. D. Philpot, "Bathymetric mapping with passive multispectral imagery," *Appl. Opt.*, vol. 28, no. 8, pp. 1569–1578, Apr. 1989.

[5] Z. P. Lee, K. L. Carder, R. F. Chen, and T. G. Peacock, "Properties of the water column and bottom derived from AVIRIS data," *J. Geophys. Res.*, vol. 106, no. C6, pp. 11 639–11 652, 2001.

[6] C. D. Mobley, L. K. Sundman, C. O. Davis, J. H. Bowles, T. V. Downes, R. A. Leathers, M. J. Montes, W. P. Bissett, D. D. R. Kohler, R. P. Reid, E. M. Louchard, and A. Gleason, "Interpretation of hyperspectral remote-sensing imagery by spectrum matching and look-up tables," *Appl. Opt.*, vol. 44, no. 17, pp. 3576–3592, Jun. 2005.

[7] A. G. Dekker, S. R. Phinn, J. Anstee, P. Bissett, V. E. Brando, B. Casey, P. Fearns, Z. P. Lee, J. Hedley, W. Klonowski, M. Lynch, M. Lyons, C. Mobley, and C. Roelfsema, "Intercomparison of shallow water bathymetry, hydro-optics, benthos mapping techniques in Australian and Caribbean coastal environments," *Limnol. Oceanogr.-Methods*, vol. 9, pp. 396–425, Sep. 2011.

[8] V. E. Brando, J. M. Ansteea, M. Wettlea, A. G. Dekkera, S. R. Phinnb, and C. Roelfsemab, "A physics based retrieval and quality assessment of bathymetry from suboptimal hyperspectral data," *Remote Sens. Environ.*, vol. 113, no. 4, pp. 755–770, Apr. 2009.

[9] W. M. Klonowski, P. R. Fearns, and M. J. Lynch, "Retrieving key benthic cover types and bathymetry from hyperspectral imagery," *J. Appl. Remote Sens.*, vol. 1, no. 1, p. 011505, Jan. 2007.

[10] J. A. Goodman, Z. P. Lee, and S. L. Ustin, "Influence of atmospheric and sea-surface corrections on retrieval of bottom depth and reflectance using a semi-analytical model, a case study in Kaneohe Bay, Hawaii," *Appl. Opt.*, vol. 47, no. 28, pp. F1–F11, Oct. 2008.

[11] Z. P. Lee, B. Casey, R. Arnone, A. Weidemann, R. Parsons, M. J. Montes, B.-C. Gao, W. Goode, C. Davis, and J. Dye, "Water and bottom properties of a coastal environment derived from Hyperion data measured from the EO-1 spacecraft platform," *J. Appl. Remote Sens.*, vol. 1, no. 1, p. 011502, Dec. 2007.

[12] R. P. Stumpf, K. Holderied, and M. Sinclair, "Determination of water depth with high-resolution satellite imagery over variable bottom types," *Limnol. Oceanogr.*, vol. 48, no. 1, pp. 547–556, Jan. 2003.

[13] Z. P. Lee, K. L. Carder, C. D. Mobley, R. G. Steward, and J. S. Patch, "Hyperspectral remote sensing for shallow waters, 2. Deriving bottom

depths and water properties by optimization," *Appl. Opt.*, vol. 38, no. 18, pp. 3831–3843, Jun. 1999.

[14] Z. P. Lee and K. L. Carder, "Effect of spectral band numbers on the retrieval of water column and bottom properties from ocean color data," *Appl. Opt.*, vol. 41, no. 12, pp. 2191–2201, Apr. 2002.

[15] E. J. Hochberg and M. J. Atkinson, "Capabilities of remote sensors to classify coral, algae, sand as pure and mixed spectra," *Remote Sens. Environ.*, vol. 85, no. 2, pp. 174–189, May 2003.

[16] Z. P. Lee, K. L. Carder, C. D. Mobley, R. G. Steward, and J. S. Patch, "Hyperspectral remote sensing for shallow waters. 1. A semianalytical model," *Appl. Opt.*, vol. 37, no. 27, pp. 6329–6338, Sep. 1998.

[17] C. D. Mobley, *Hydrolight 3.0 Users' Guide*.   Menlo Park, CA: SRI Int., 1995.

[18] H. R. Gordon, O. B. Brown, R. H. Evans, J. W. Brown, R. C. Smith, K. S. Baker, and D. K. Clark, "A semianalytic radiance model of ocean color," *J. Geophys. Res.*, vol. 93, no. D9, pp. 10 909–10 924, Sep. 1988.

[19] C. D. Mobley, *Light and Water, Radiative Transfer in Natural Waters*. New York: Academic, 1994.

[20] Z. P. Lee, K. L. Carder, and K. P. Du, "Effects of molecular and particle scatterings on model parameters for remote-sensing reflectance," *Appl. Opt.*, vol. 43, no. 25, pp. 4957–4964, Sep. 2004.

[21] R. Pope and E. Fry, "Absorption spectrum (380–700 nm) of pure waters, II. Integrating cavity measurements," *Appl. Opt.*, vol. 36, no. 33, pp. 8710–8723, Nov. 1997.

[22] A. Morel, "Optical properties of pure water and pure sea water," in *Optical Aspects of Oceanography*, N. G. Jerlov and E. S. Nielsen, Eds. New York: Academic, 1974, pp. 1–24.

[23] "Remote sensing of inherent optical properties, fundamentals, tests of algorithms, applications," in *Proc. Rep. Int. Ocean-Colour Coordinating Grp.*, Z.-P. Lee, Ed., Dartmouth, Canada, 2006, vol. 5, p. 126.

[24] G. M. Hale and M. R. Querry, "Optical constants of water in the 200 nm to 200 μm wavelength region," *Appl. Opt.*, vol. 12, no. 3, pp. 555–563, Mar. 1973.

[25] Z. P. Lee, K. L. Carder, and R. Arnone, "Deriving inherent optical properties from water color, a multi-band quasi-analytical algorithm for optically deep waters," *Appl. Opt.*, vol. 41, no. 27, pp. 5755–5772, Sep. 2002.

[26] L. S. Lasdon, A. D. Waren, A. Jain, and M. Ratner, "Design and Testing of Generalized Reduced Gradient Code for Nonlinear Programming," Stanford Univ., Stanford, CA, Tech. Rep. SOL 76-3, pp. 1–51, 1976.

[27] D. Fylstra, L. Lasdon, J. Watson, and A. Waren, "Design and use of the Microsoft Excel Solver," *Interfaces*, vol. 28, no. 5, pp. 29–55, Sep./Oct. 1998.

[28] Z. P. Lee, "Applying narrowband remote-sensing reflectance models to wideband data," *Appl. Opt.*, vol. 48, no. 17, pp. 3177–3183, Jun. 2009.

[29] K. R. Lee, A. M. Kim, R. C. Olsen, and F. A. Kruse, "Determination of bottom-type and bathymetry using WorldView-2," in *Proc. SPIE Ocean Sens. Monitoring III*, Orlando, FL, 2011, pp. 80300D-1–80300D-12.

[30] M. J. Loomis, "Depth derivation from the WorldView-2 satellite using hyperspectral imagery," M.S. thesis, Naval Postgraduate School, Monterey, CA, 2009.

[31] P. J. Werdell and C. S. Roesler, "Remote assessment of benthic substrate composition in shallow waters using multispectral reflectance," *Limnol. Oceanogr.*, vol. 48, no. 1, pp. 557–567, 2003.

Zhongping Lee received the B.S. degree in optical physics from Sichuan University, Chengdu, China, in 1984, the M.S. degree in laser application from the Ocean University of China, Qingdao, China, in 1987, and the Ph. D. degree in ocean-color remote sensing from the University of South Florida, St. Petersburg, in 1994.

He is a Professor with the Department of Environmental, Earth, and Ocean Sciences, University of Massachusetts, Boston. He has conducted research studies in ocean optics and ocean-color remote sensing for both optically deep and shallow waters and has developed widely used models and algorithms for retrieving important environmental properties from the observation of water color.

Alan Weidemann received the Ph. D. degree from the University of Rochester, Rochester, NY, in 1985.

Since 1985, he has been working on ocean optics with the Naval Ocean Research and Development Activity/Naval Research Laboratory, Stennis Space Center, MS. His main work has been in the area of *in situ* bio-optical properties and their impact on the light field of aquatic environments and on active and passive light propagation. He also works on the retrieval of optical properties from high-resolution remote sensing in rivers and coastal waters.

Robert Arnone retired as the Branch Head of the Ocean Processes Branch, Naval Research Laboratory, Stennis Space Center, MS. He is a Research Professor with the Department of Marine Science, The University of Southern Mississippi, Stennis Space Center. His research is directed at satellite ocean-color remote sensing and characterizing bio-optical processes of the ocean and coupling satellite bio-optics with ecosystem ocean models. He is currently coordinating the calibration of the JPSS satellite ocean products for NOAA and serves on numerous NASA and Navy ocean-color steering teams. He has organized and led national and international sea-going oceanographic expeditions throughout the world and authored over 100 publications.